Military Technical College
Kobry El-Kobbah,
Cairo, Egypt.

17th International Conference on Applied Mechanics and Mechanical Engineering.

MICROSTRUCTURAL AND THERMAL INVESTIGATIONS OF CU-AL-MN-NI SHAPE MEMORY ALLOYS

C. A. Canbay[a] and V. Sampath[b]

ABSTRACT

Shape memory alloys manifest two distinct characteristics, namely shape memory effect and superelastic effect. They are used in a wide variety of engineering, medical and commercial applications. The use of shape memory alloys in a particular application depends on the shape memory characteristics, viz., shape recovery strain and transformation temperatures. The martensitic transformation and its reversibility form the basis of these functional properties. The transformation temperatures are much influenced by alloying addition, grain-refinement, thermomechanical treatment, etc. In this work, the effect of composition in general, and that of nickel in particular, on the microstructure and transformation temperatures and thermodynamic parameters have been explored. The microstructural and phase analyses were carried out by optical microscopy and x-ray diffraction, respectively. The thermodynamic quantities/parameters, such as enthalpy and entropy associated with the transformations as well as the transformation temperatures, were determined by differential scanning calorimetry. The phase analyses were also carried out by thermogravimetry and differential thermal analysis. The results have been analysed and discussed in this paper.

KEYWORDS

Shape memory alloys; Shape memory characteristics; Transformation temperatures; Microstructural analysis; Phase analysis.

---

[a] Department of Physics, Faculty of Science, University of Firat, Elazig, TR-23119, Turkey.
[b] Department of Metallurgical and Materials Engineering, Indian Institute of Technology Madras, Chennai-600 036, India.

INTRODUCTION

Shape memory alloys possess the unique properties of shape memory effect and superelastic effect. The reversibility of martensitic transformation is attributed to these characteristics. Copper-based shape memory alloys are preferred to Ni-Ti shape memory alloys for a number of reasons: a. easier to produce; b. easier to process; c. cheaper than Ni-Ti SMAs; d. some alloys show shape memory characteristics that are comparable to Ni-Ti SMAs; e. show higher transformation temperatures than N-Ti SMAs. There are also some limitations and drawbacks associated with copper-based SMAs: a. coarse grains leading brittleness; b. tendency to age at lower temperatures causing stabilization of martensite; c. ordering causing brittleness[1-6].

There are many ways by which the properties are improved and the drawbacks of the binary and ternary copper-based alloys are overcome: a. alloying to increase/decrease transformation temperatures; b. grain-refinement to increase ductility; c. adoption of different quenching techniques to overcome thermal stabilization [6-9].

Cu-Al-Mn SMAs are known as cryogenic shape memory alloys exhibiting lower transformation temperatures. They are used as guidewires in surgical procedures. If they are to be used in other applications, then their transformation temperatures are to be modified. In this paper, therefore, the use of nickel as a quaternary alloying addition has been attempted with a view to modifying the microstructural features and thermodynamic parameters, and thereby bring about variation in the characteristic transformation temperatures [10-14].

EXPERIMENTAL

Cu-Al-Mn-Ni shape memory alloys with the following nominal compositions were produced by arc melting in an argon atmosphere: Cu-24.78 Al-4.83 Mn-1.32 Ni (at.%), Cu-21.4 Al-4.48 Mn-1.5 Ni (at.%), Cu-26.11 Al-4.27 Mn-1.54 Ni (at.%) and Cu-26 Al-4.33 Mn-1.44 Ni (at.%). The alloys were designated as: A, B, C and D, respectively. The specimens were solution treated at 1173 K for 1 h and quenched in iced-brine water. The chemical compositions of the alloys were examined by LEO evo 40 Model energy dispersive X-ray (EDX) analyser. The characteristic transformation temperatures were determined using a Shimadzu DSC-60A differential scanning calorimeter at a heating/cooling rate of 20 K/min. The phase transitions occurring in the alloys at high temperatures were observed using a Shimadzu DTG-60AH differential thermogravimeter. Phase analysis was carried out on a Rigaku RadB-DMAX II X-ray diffractometer using CuK_{α} radiation at room temperature. The surfaces of the samples were cleaned by an etching solution for optical microscope analysis and microstructural observations were made using a Nikon MA200 optical microscope.

RESULTS AND DISCUSSION

Thermal Analysis of the SMAs

The DSC analysis was carried out on the alloy samples so as to determine the characteristic transformation temperatures of the samples at a heating/cooling rate of 20 K/min. The characteristic transformation temperatures A_s, A_f, M_s and M_f and the hysteresis width (A_f-M_s) of the samples are given in Table 1. As mentioned in literature alloying elements in SMAs affect the transformation temperatures and the modified values based on our experiments on differential scanning calorimetry are given in Fig.1. [1-14]. The hysteresis values also changed according to these temperatures. The thermodynamic parameters, such as enthalpy, entropy and equilibrium temperatures of the samples, are given in Table 1. The enthalpy values of the samples were determined using the tangent method, while the entropy and equilibrium temperatures were calculated following the methods adopted by other researchers [15-21]. The equilibrium temperature (T_0) between the parent phase and martensite phase was calculated based on the following relations when the Gibbs free energy (G) of both phases are equalized [22, 23]:

$$\Delta G^{M\to A}(T_0) = G^A(T_0) - G^M(T_0)$$

$$= (H^A - T_0 S^A) - (H^M - T_0 S^M)$$

$$= \Delta H^{M\to A} - T_0 \Delta S^{M\to A} \quad (1)$$

or

$$\Delta G^{A\to M}(T_0) = G^M(T_0) - G^A(T_0)$$

$$= (H^M - T_0 S^M) - (H^A - T_0 S^A)$$

$$= \Delta H^{A\to M} - T_0 \Delta S^{A\to M} \quad (2)$$

In addition to this the Gibbs free energies of the austenite and martensite phases are equal at $T=T_0$ and can be expressed as follows [21]:

$$T_0 = \frac{\Delta H^{M\to A}}{\Delta S^{M\to A}} \text{ or } T_0 = \frac{\Delta H^{A\to M}}{\Delta S^{A\to M}} \quad (3)$$

On the other hand, the equilibrium temperature between the austenite and martensite phase transformation can be calculated by [24]:

$$T_0 = \frac{(A_f + M_s)}{2} \quad (4)$$

The phase transition tendencies of the samples are shown in Fig. 2. The different stages in the phase transition of the samples on heating are given by: i) *A2→B2* transition, ii) *B2→L2₁* transition, iii) *L2₁→*9R or 18R transition. The DTA curves of the

samples refer to; *A2→B2* transition in the temperature interval 700-900 K, *B2→L2₁* transition between 300-450 K and *L2₁*→9R or 18R transition at room temperature [7-16]. The curves pertaining to each of the alloys as obtained from the DTA analysis is different due to the fact that these alloys have different alloy contents.

Microstructural and Phase Analyses of SMAs

The XRD analysis of the samples was made at room temperature and the lattice parameters of the alloys are given by: a = 4.494 Å; b = 5.189Å; and c = 46.610 Å. The ratio *a/b* was calculated to be 0.86. This confirms that the parent phase is ordered and that it has a long period stacking order (LPSO) structure. This means that during the rapid cooling the high temperature *β*-phase expands to an *L2₁* ordered structure and further transforms to a martensite phase at room temperature. The diffraction peaks of the samples are given in Fig. 3. The major diffraction peaks corresponding to the martensite phase in all the samples were found to be (0022), (1210) and (2012) [25-27].

The average crystallite size (*D*) of each sample can be determined by Debye-Scherrer equation [28, 29].

$$D = \frac{0.9\lambda}{B_{½}\cos\theta} \tag{5}$$

where *λ* is the wavelength of the X-ray (CuK$_\alpha$ radiation), *B* is the peak full width at half maximum, and *θ* is the Bragg angle. The calculated crystallite sizes of the samples are 18.09, 19.33, 21.6 and 28.3 nm, respectively.

Optical microscopic observations were made at room temperature to support the results of XRD analysis. These observations bring to light that the parent phase is martensite as shown in Fig.4. Martensite variants, grains and grain boundaries occuring in the microstructure of the samples are clear and the orientations of martensite variants are different.

CONCLUSIONS

The martensitic transformation in Cu-Al-Mn-Ni SMAs was investigated. The transformation temperatures, phase transitions and microstructural features of Cu-Al-Mn-Ni system with different compositions were studied by differential thermal analysis and optical microscopy.

Differential scanning calorimetry was used to investigate the forward-reverse transformation temperatures, enthalpy and entropy values as well as the equilibrium temperatures of the samples. The calculated enthalpy and entropy values for the martensite to austenite transformation vary depending upon the composition of the alloys. A comparison of the phase transition temperatures of the alloys studied reveals that the temperatures for the ordered transitions are influenced more by the Al content rather than the Mn content. In addition, it was found that the quaternary

addition (Ni) affects the β(A2)→β_2(B2)→β_1($L2_1$) transition temperatures. The diffraction patterns of the SMAs show the presence of β'_1 martensite, which corresponds to the 18R structure at room temperature. The optical microscopic images of the alloy samples support the XRD results and reveal the presence of β'_1 martensite at room temperature.

ACKNOWLEDGEMENTS

This work was financially supported by FÜBAP, Project No: FF.15.14.

REFERENCES

[1] H.J. Jiang, S.Cao, C.B. Ke, X. Ma, X.P. Zhang, Mater. Lett. **100**, (2013) 74.
[2] M. Izadinia, K. Dehghani, Trans. Nonferrous Met. Soc. China. **21**, (2011) 2037
[3] J. Yu-qin, W. Yu-hua, L. Ming, H. Jia-qiang, T. Jin, Trans. Nonferrous Met. Soc. China. **19**, (2009) 616.
[4] L. Yan, C. Lishan, Z. Yanjun, Y. Dazhi: Mater. Lett. **51**, (2001) 73.
[5] X.L. Meng, Y.F. Zheng, W. Cai, L.C. Zhao, J. Alloy. Compd. **372**, (2004) 180.
[6] Z. Karagoz, C. Aksu Canbay, J. Therm. Anal. Calorim., DOI: 10.1007/s10973-013-3145-9.
[7] Y. Sutou, T. Omori, R. Kainuma, K. Ishida, Grain size dependence of pseudoelasticity in polycrystalline Cu–Al–Mn-based shape memory sheets. Acta Mater. 61, 3842–3850 (2013).
[8] Q. Wang, D. Lu, C. Cui, N. Yan, Q. Wang, Fabrication and internal friction behaviors of novel porous CuAlMn shape memory alloy filled with polystyrene. Mater. Lett. 92, 82–85(2013).
[9] Development of a Cu-Al-Mn Shape-Memory Alloy and its Application to an Ingrown Toenail Correcting Clip. Furukawa Rev 41: 22–4 (2012).
[10] X. Lu, F. Chen, W. Li, Y. Zheng, Effect of Ce addition on the microstructure and damping properties of Cu–Al–Mn shape memory alloys. J. Alloys Compd. 480, 608–611 (2009).
[11] N. Zarubova, V. Novak, Phase stability of CuAlMn shape memory alloys. Mater. Sci. Eng. A 378, 216–221 (2004).
[12] Y.Q. Jiao, Y.H. Wen, N. Li, J.Q. He, J. Teng, Effect of solution treatment on damping capacity and shape memory effect of a CuAlMn alloy. J. Alloys Compd. 491, 627–630 (2010).
[13] R. Kainuma, N. Satoh, X.J. Liu, I. Ohnuma, K. Ishida, Phase equilibria and heusler phase stability in Cu-rich portion of the Cu–Al–Mn system. J. Alloys Compd. 266, 191–200 (1998).
[14] Y. Jiao, Y. Wen, N. Li, J. He, J. Teng, Effect of environmental temperature on damping capacity of Cu–Al–Mn alloy. Trans. Nonferrous Met. Soc. China 19, 616–619 (2009).
[15] R.A. Portier, P. Ochin, A. Pasko, G.E. Monastyrsky, A.V. Gilchuk, V.I. Kolomytsev, and Y.N. Koval, J. Alloy. Compd., DOI: 10.1016/j.jallcom.2012.02.145.

[16] C.Aksu Canbay, A. Aydogdu, J. Therm. Anal. Calorim., DOI: 10.1007/s10973-012-2792-6
[17] N. Suresh, U. Ramamurty, J. Alloy. Compd. **449**, (2008) 113.
[18] G.K.Kannarpady, A. Bhattacharyya, S.Pulnev, I. Vahni, J. Alloy. Compd. **425**, (2006) 112.
[19] J. Rodriguez-Aseguinoloaza, I. Ruiz-Larrea, M.L.No, A. Lopez-Echarri, J. M. San Juan, Acta Mater. **58**, (2008) 3711.
[20] H. Kato, Y.Yasuda, K. Sasaki: Acta Mater. **59**, (2011) 3955.
[21] R. J.Salzbrenner, M. Cohen, Acta Metall. **27,** (1979) 739.
[22] J. Ortin, A. Planes, Acta Metall. **37**, (1988) 1873.
[23] E. Obrado, L. Manosa, Phys. IV. France 7, Colloque C5, Supplement au J. Phys. III de Novembre (1997).
[24] M.O. Prado, P.M. Decorte, F. Lovey, Scripta Metall. Mater. **33**, (1995) 878.
[25] R. Kainuma, S.Takahashi, K. Ishida, Metall. Mater. Trans. A **27**, (1996) 2187.
[26] U.S. Mallik, V. Sampath, J. Alloy. Compd. **469**, (2009) 156.
[27] S.Stanciu, L.G. Bujoreanu, Mat. Sci. Eng. A. **481-482**, (2008) 494.
[28] Suresh N, Ramamurty U (2008) Aging response and its effect on the functional properties of Cu-Al-Ni shape memory alloys. J Alloy. Compd. 449:113-118.
[29] Sonia D, Rotaru P, Rizescu S, Bizdoaca N.G (DOI: 10.1007/s10973-012-2369-4) Thermal study of a shape memory alloy (SMA) spring actuator designed to insure the motion of a barrier structure. J Therm. Anal Calorim. 2013:111-1255-1262.

Table 1. Transformation temperatures and hysteresis values of alloys obtained at a heating/cooling rate of 20 K/min.

Alloy ID	A_s (K)	A_f (K)	M_s K)	M_f (K)	(A_f-M_s) (K)	T_0 (K)	$\Delta H_{M\rightarrow A}$ J/g)	$\Delta S_{M\rightarrow A}$ (J/g K)
A	379.07	398.09	357.81	338.71	40.28	377.55	8.53	0.022
B	388.76	403.78	364.65	338.95	39.13	384.21	8.07	0.021
C	345.76	369.03	325.94	315.22	43.09	347.48	8.91	0.025
D	330.05	346.11	296.48	286.76	49.63	321.29	6.13	0.019

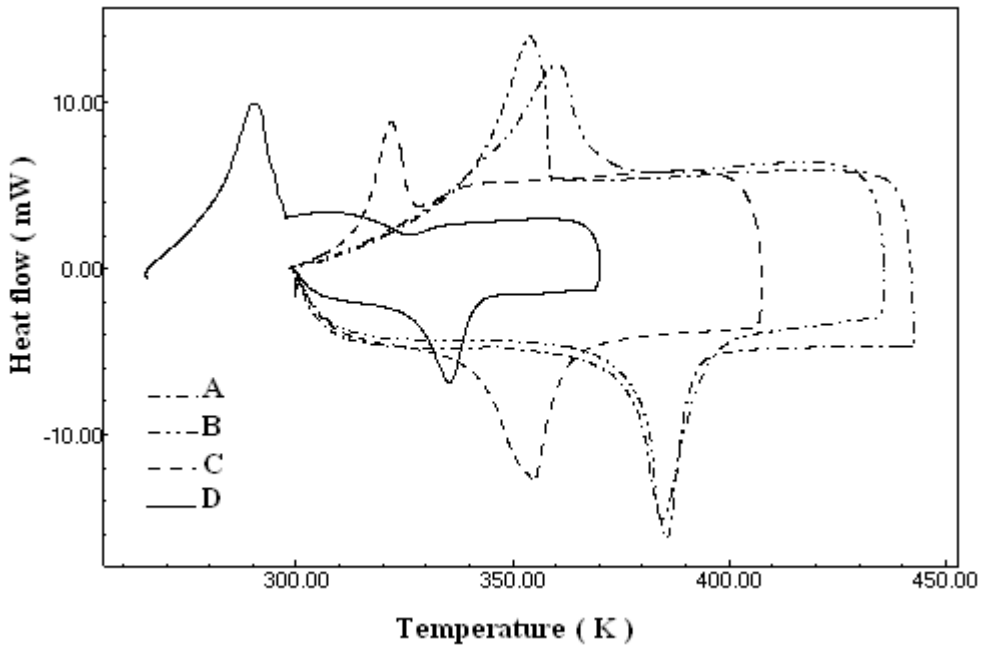

Fig. 1. DSC curves for samples A, B, C and D.

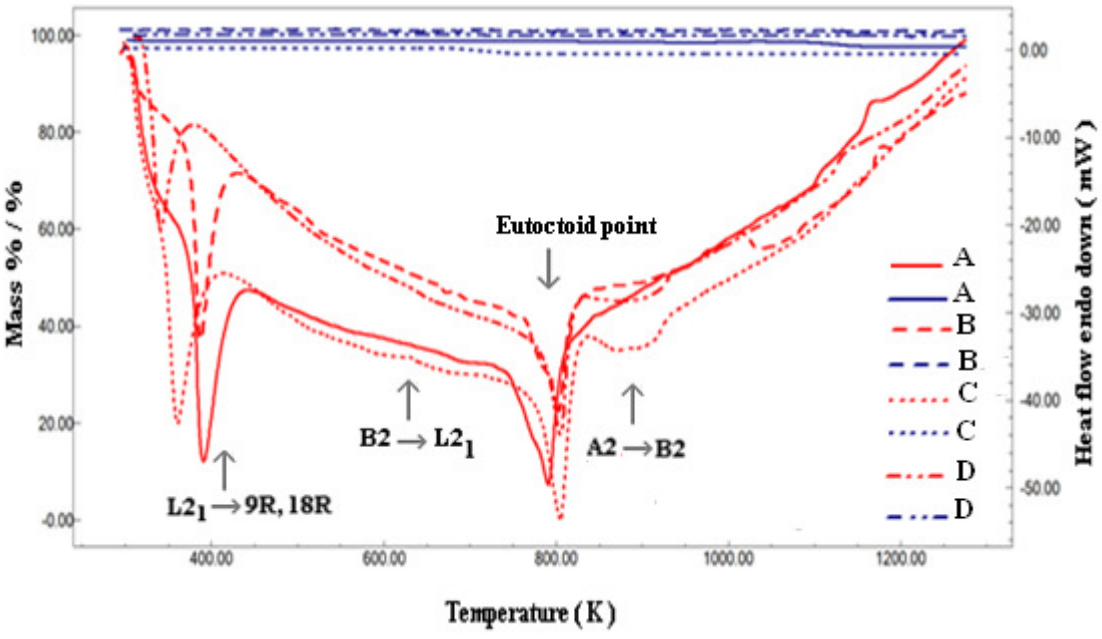

Fig. 2. TG/DTA curves for samples A, B, C and D.

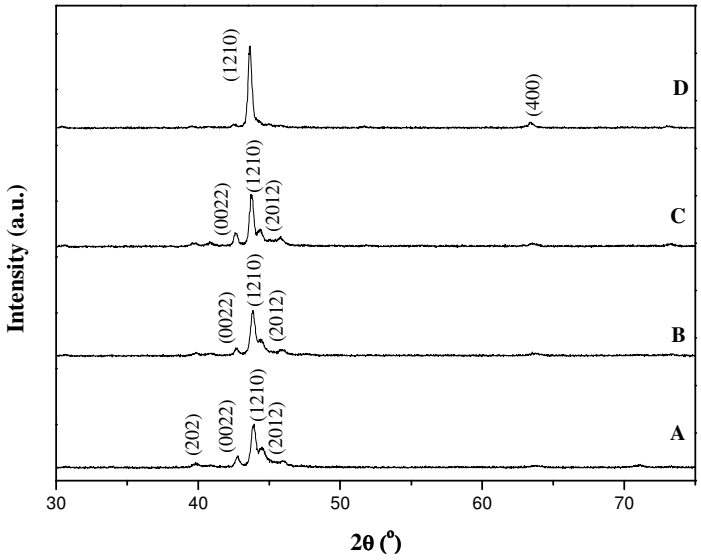

Fig.3. X-Ray diffraction patterns of samples A, B, C and D.

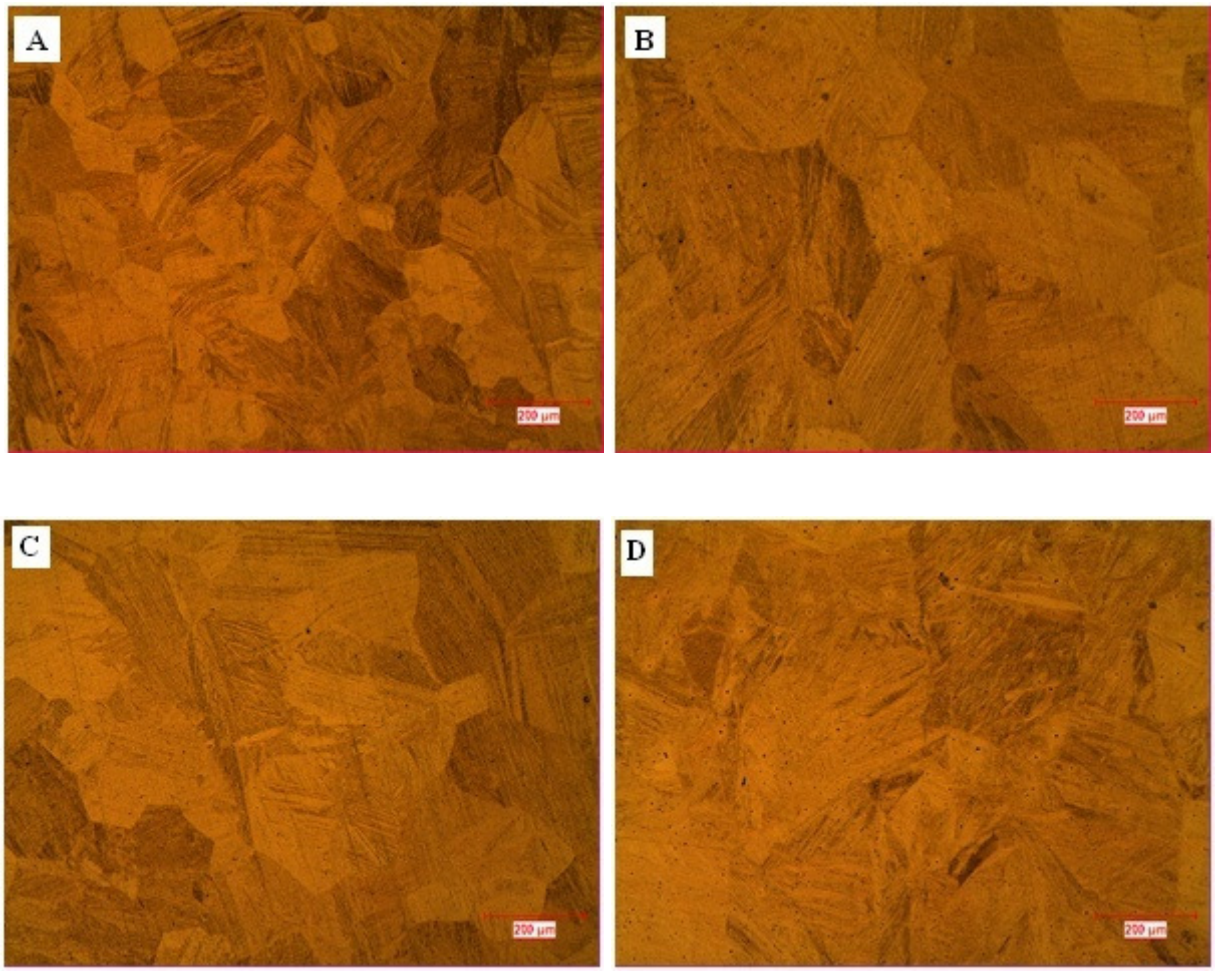

Fig.4. Optical micrographs of samples A, B, C and D.